Rotational relaxation in ultracold CO+He collisions

P. M. Florian, M. Hoster, and R. C. Forrey
Penn State University, Berks-Lehigh Valley College, Reading, Pennsylvania 19610-6009, USA
(Received 26 March 2004; published 22 September 2004)

Cold and ultracold collisions involving rotationally hot CO molecules are investigated using quantum mechanical coupled channel, coupled states, and effective potential scattering formulations. Quenching rate coefficients are given for initial rotational levels near the dissociation threshold. The stability of the CO "super rotors" against collisional decay is compared to previous investigations involving homonuclear molecules. It is found that quasiresonant transitions provide a significantly stronger contribution to the total relaxation rate than in the comparable case of O_2. As in the case of H_2, sharp structures in the distribution of total quenching rate coefficients are found at rotational levels where quasiresonant scattering is not allowed.

DOI: 10.1103/PhysRevA.70.032709 PACS number(s): 34.50.Ez

I. INTRODUCTION

Experimental schemes to cool and trap neutral polar molecules using a time-varying electric field have been proposed [1,2] and recently realized [3]. Meijer and co-workers have applied the so-called Stark decelerator to slow down metastable CO molecules [1]. Schemes to produce diatomic molecules in highly excited rotational states have also been proposed [4,5] and recently realized [6]. Theoretical studies have suggested that the collisional dynamics of such rotationally hot molecules would be particularly interesting at low temperatures [7–11]. These studies concentrated on homonuclear diatomic molecules where it was found that quasiresonant vibration-rotation (QRVR) transitions contributed significantly in quenching the highly rotationally excited molecules. Another recent investigation showed that QRVR transitions have a neglible effect on the relaxation of rotationally hot oxygen molecules and that the quenching is very efficient for all rotational levels and dominated by pure rotational deexcitation [12]. Each of the theoretical investigations [7–12] assumed a helium atom collision partner. Helium buffer gas cooling [13] has proven to be an effective technique for loading molecules into a magnetic trap [14] and it has recently been shown that the cooling technique may be applied to a beam of molecules [15]. Therefore, collisions involving helium atoms are of considerable interest in ultracold molecular physics. In this work, we perform relaxation studies for helium collisions with CO. We compute an extensive amount of collisional data that may be used as a point of comparison to the molecular hydrogen and oxygen systems studied previously and investigate whether heteronuclear molecules introduce any interesting variations to the low temperature collisional dynamics seen in rotationally excited homonuclear molecules. Because heteronuclear polar molecules like CO possess an electric dipole moment, the radiative decay signal would contain information about the collisions. With the rapid advances in experimental techniques mentioned above [1–6,13–15] it is possible that CO+He may turn out to be an ideal system for experimental investigations of rotational relaxation in ultracold atom-diatom collisions.

Vibrational relaxation in ultracold CO+He collisions has been studied for both isotopes of helium [16–18]. Strong resonances were predicted [16,17] and the relative efficiency of the processes involving exchange of a double or single quantum of vibrational energy was studied [18]. There have also been a number of theoretical [16–20] and experimental [21,22] investigations of vibrational relaxation for this system at higher temperatures. Excellent agreement between theory and experiment has been established for temperatures between 35 and 1500 K. The vibrational relaxation studies have considered vibrational levels as high as $v=2$ [18] and rotational levels as high as $j=40$ [20], where v and j are the vibrational and rotational quantum numbers of the CO molecule. Here, we consider all bound rotational levels within the first five vibrational manifolds. At these low vibrations, the molecule can support rotational levels up to $j=230$ or so before dissociating. It would be hopeless to attempt to perform fully quantum mechanical coupled channel (CC) calculations at such large values of j. Therefore, we will employ a decoupling approximation to obtain the desired large-j scattering data. It was shown in the case of H_2 and O_2 [12] that both the coupled states (CS) and the effective potential (EP) approximations were adequate for obtaining qualitatively reliable cross sections in the limit of ultracold collisions. By qualitatively reliable, we mean that the shape of a cross section or rate coefficient curve as a function of v or j is correct, even though the overall magnitude of the curve may be off by a small factor [12]. This situation is entirely satisfactory considering that inaccuracies in the potential energy surface typically introduce a comparable amount of error. If more quantitative accuracy is desired, it is possible to renormalize the distributions using the CC results. In this work, we will again test the CS and EP approximations against the more accurate CC results in cases where it is possible to perform the computationally intensive CC calculations. After determining the accuracy of the decoupling approximations, we compute cross sections and rate coefficients for ultracold He+CO collisions with initial rotational levels ranging all the way to dissociation. For a few special cases of initial diatomic states, we extend the investigations to include a range of translational temperatures.

II. THEORY

The CC, CS, and EP formulations have been given previously [23–26] so we provide only a brief review. The atom-

diatom Hamiltonian in the center of mass frame is given by

$$H = -\frac{1}{2m}\nabla_r^2 - \frac{1}{2\mu}\nabla_R^2 + v(r) + V_I(r,R,\theta), \tag{1}$$

where r is the distance between the carbon and oxygen atoms, R is the distance between the helium atom and the center of mass of the molecule, θ is the angle between $\boldsymbol{r}$ and $\boldsymbol{R}$, m is the reduced mass of the molecule, and μ is the reduced mass of the helium atom with respect to the molecule. The three dimensional potential energy surface is separated into a diatomic potential $v(\boldsymbol{r})$ and an interaction potential $V_I(r,R,\theta)$. The diatomic Schrödinger equation

$$\left[\frac{1}{2m}\frac{d^2}{dr^2} - \frac{j(j+1)}{2m\ r^2} - v(r) + \epsilon_{vj}\right]\chi_{vj}(r) = 0 \tag{2}$$

is solved by expanding the rovibrational wave function $\chi_{vj}(r)$ in a Sturmian basis set. Each scattering formulation then requires the solution of a set of coupled equations of the form

$$\left[\frac{d^2}{dR^2} - \frac{l_m(l_m+1)}{R^2} + 2\mu E_m\right] C_m(R) = \sum_n C_n(R)\langle\phi_m|U_I|\phi_n\rangle, \tag{3}$$

where E_m is the translational energy and l_m is the orbital angular momentum in the mth channel. For the CC formulation, the index on the channel function ϕ_m is assumed to denote some combination of the quantum numbers (v,j,l), whereas for the CS and EP formulations, the index denotes only (v,j). The reduced interaction potential U_I is expanded in Legendre polynomials,

$$U_I(\boldsymbol{R},\boldsymbol{r},\theta) = 2\mu V_I(\boldsymbol{R},\boldsymbol{r},\theta) = \sum_{\lambda=0}^{\infty} U_\lambda(\boldsymbol{R},\boldsymbol{r})P_\lambda(\cos\ \theta) \tag{4}$$

and the solution to Eq. (3) is matched asymptotically to free waves to obtain the scattering matrix. The CS and EP formulations assume that the orbital angular momentum of the atom is decoupled from the rotational angular momentum of the diatom during the collision. At low values of j and l, this assumption may not be valid, however, the approximation generally improves as j is increased [26]. For a basis set of rovibrational eigenstates χ_{vj}, the respective matrix elements of the reduced interaction potential energy are given by

$$\langle vjl|U_I|v'j'l'\rangle = \sum_{\lambda=0}^{\lambda_{max}} (-1)^{j+j'-J}[(2j+1)(2j'+1)(2l+1)(2l'+1)]^{1/2} \times \begin{Bmatrix} J & l & j \\ \lambda & j' & l' \end{Bmatrix} \begin{pmatrix} j' & \lambda & j \\ 0 & 0 & 0 \end{pmatrix} \times \begin{pmatrix} l' & \lambda & l \\ 0 & 0 & 0 \end{pmatrix} \langle\chi_{vj}|U_\lambda|\chi_{v'j'}\rangle, \tag{5}$$

$$\langle vj\Omega|U_I|v'j'\Omega\rangle = \sum_{\lambda=0}^{\lambda_{max}} (-1)^{\Omega}[(2j+1)(2j'+1)]^{1/2} \times \begin{pmatrix} j' & \lambda & j \\ 0 & 0 & 0 \end{pmatrix} \begin{pmatrix} j' & \lambda & j \\ \Omega & 0 & -\Omega \end{pmatrix} \langle\chi_{vj}|U_\lambda|\chi_{v'j'}\rangle, \tag{6}$$

$$\langle vj|U_I|v'j'\rangle = \sum_{\lambda=0}^{\lambda_{max}} \left[\frac{(-1)^{j+j'+|j-j'|}}{(2\lambda+1)}\sqrt{(2j+1)(2j'+1)}\right]^{1/2} \times \begin{pmatrix} j' & \lambda & j \\ 0 & 0 & 0 \end{pmatrix} \langle\chi_{vj}|U_\lambda|\chi_{v'j'}\rangle \tag{7}$$

for the CC, CS, and EP formulations. The $(\cdots)$ denotes a 3-j symbol and $\{\cdots\}$ denotes a 6-j symbol. The CS formulation requires a set of calculations for each value of diatomic angular momentum projection quantum number Ω whereas the EP formulation preaverages over the projection states and is independent of Ω. The respective CC, CS, and EP cross sections are given by [23–26]

$$\sigma_{vj\to v'j'} = \frac{\pi}{2\mu E_{vj}(2j+1)}\sum_{J=0}^{\infty}(2J+1)\sum_{l=|J-j|}^{|J+j|}\sum_{l'=|J-j'|}^{|J+j'|}|\delta_{jj'}\delta_{ll'}\delta_{vv'} - S^J_{vjl;v'j'l'}|^2, \tag{8}$$

$$\sigma_{vj\to v'j'} = \frac{\pi}{2\mu E_{vj}(2j+1)}\sum_{J=0}^{\infty}(2J+1)\sum_{\Omega=0}^{\Omega_{max}}(2-\delta_{\Omega 0})|\delta_{jj'}\delta_{vv'} - S^{J\Omega}_{vj;v'j'}|^2, \tag{9}$$

$$\sigma_{vj\to v'j'} = \frac{\pi}{2\mu E_{vj}}\sum_{l=0}^{\infty}(2l+1)|\delta_{jj'}\delta_{vv'} - S^l_{vj;v'j'}|^2. \tag{10}$$

The quantum mechanical scattering calculations were carried out for each of the CC, EP, and CS formulations using the nonreactive scattering program MOLSCAT [27] suitably adapted to the present system. The interaction potential energy surface of Heijmen *et al.* [28] was used for all calculations presented in this work. This potential allows for stretching of the CO bond and is able to reproduce the bound state energies of the He-CO complex. For the diatomic molecule, we used the extended Rydberg potential [29] employed by Balakrishnan *et al.* [16]. A basis set consisting of 50 Hermite polynomials for each rotational symmetry was used to represent the rovibrational wave functions. For the CS calculations, we have found it convenient to restrict the projection quantum number Ω to be zero. This allows a considerable speedup in efficiency with computation times that are comparable to the EP calculations. As in the case of O_2 [12] this procedure will typically shift the overall magnitude of the cross section or rate coefficient curves without altering the shape or any structure that they may contain. It also does not introduce any significant loss of accuracy beyond that which is already introduced by the decoupling approximation to begin with. We have also adopted the l-labeled variant of the CS approximation originally proposed by McGuire and

Khouri [24] which assumes that the diagonal eigenvalue of the orbital angular momentum operator $\hat{l}^2$ is approximated by $l(l+1)$ where l is a conserved quantum number. The collisional rate coefficients may be obtained from the usual thermal averaging procedure

$$R_{vj\to v'j'}(T) = (8k_BT/\pi\mu)^{1/2}\frac{1}{(k_BT)^2}\int_0^\infty \sigma_{v,j\to v',j'}(E_k) \times \exp(-E_k/k_BT)E_k\, dE_k, \tag{11}$$

where T is the temperature and k_B is the Boltzmann constant. The total quenching rate coefficients $R_{vj}(T)$ are given by

$$R_{vj}(T) = \sum_{v'j'} R_{vj\to v'j'}(T). \tag{12}$$

The sum in Eq. (12) includes contributions from all possible exit channels. The total quenching rate coefficient is an important quantity in cooling and trapping experiments. Any type of deexcitation process will lead to unwanted heating of the gas and limit further cooling efforts. In the case of helium collisions with O_2, the total quenching rate coefficients were dominated for all v and j by pure rotational de-excitation contributions $j'=j-2$. QRVR transitions, which typically occur at initial j-values where rotational and vibrational motion of the diatom are near resonance and are characterized by propensity rules relating the change in v to the change in j [30], were found to be of inconsequential importance for this system [12]. By contrast, the energetically allowed QRVR $\Delta j=-2\Delta v$ transitions for He+H_2 were found to dominate the pure rotational contributions by about 5 orders of magnitude [9,11]. It is such cases, where the efficiency of rovibrational transitions is comparable to or greater than pure rotational deexcitation, that we would expect to see interesting structure in the distribution of total quenching rate coefficient with j. This is due not only to the competitive balance between the two relaxation pathways, but also to the closing of QRVR transitions that can occur for specific j values at low temperatures.

III. RESULTS

Figure 1 compares the total quenching rate coefficients for zero-temperature collisions calculated with the CC, EP, and CS scattering formulations. The molecule is initially in the $v=0$ level for each calculation with the basis set restricted to $j-10\leqslant j'\leqslant j+2$ and $v_{max}=1$. The anisotropy of the potential energy surface requires $\lambda_{max}=20$ with 40 integration nodes for the angle between the diatom and the line connecting the atom to the center of mass of the diatom. These parameters are twice those used for He+O_2 [12] which allowed CC calculations for $j\leqslant 40$ before becoming intractable. In the present case, the CC calculations become intractable for $j>20$ and a decoupling approximation such as EP or CS must be used. As in the case of He+O_2, it appears that such approximations will provide estimates for large j that are reliable to within a factor of 2.

Figure 2 shows the energy gaps between the initial and final rovibrational states of CO($v=1,j$) as a function of j.

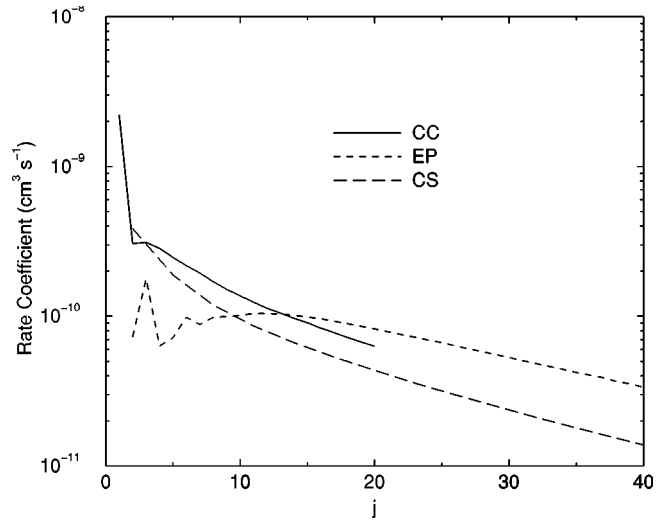

FIG. 1. Total quenching rate coefficents for He+CO($v=0,j$) in the limit of zero temperature. The curves were computed using the CC (solid line), EP (short dashed line), and CS (long dashed line) scattering formulations. For $j>20$, the CC calculations become intractable and a decoupling approximation such as EP or CS must be used. From the figure, it appears that such approximations will provide estimates for large-j that are reliable to within a factor of 2.

The boxed region on the right shows where $\Delta j=-2\Delta v$ QRVR transitions are likely to take place. Unlike the case of O_2, there exists a positive crossing point for the upward and downward curves. There also exist QRVR $\Delta j=-3\Delta v$ transitions (leftmost boxed region) that were absent in the homonuclear O_2 and H_2 cases studied previously. The positive crossing points in the boxed regions represent j values where classical trajectory calculations would generally predict the strongest correlation between Δv and Δj and therefore the

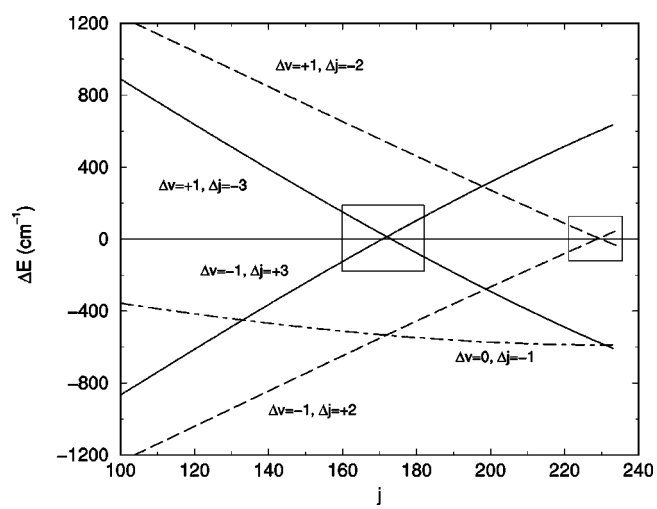

FIG. 2. Energy gaps between initial and final rovibrational states for CO($v=1,j$). The boxed regions show where QRVR transitions typically occur. In both cases, the energy gap is positive at the crossing point between the two curves. Interesting threshold behavior may be expected for cold collisions near these j values. The respective energy gaps for the crossing points are 12.8 cm^{-1} and 4.2 cm^{-1} for the $\Delta j=-3\Delta v$ and $\Delta j=-2\Delta v$ curves.

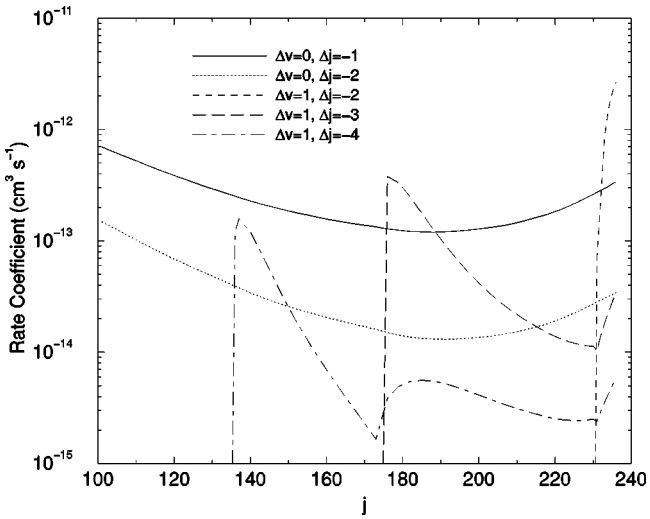

FIG. 3. State-to-state rate coefficients for He+CO($v=0,j$) in the limit of zero temperature. "Steps" occur at j values where the vibrationally upward QRVR transitions become energetically open.

largest and most specific transition efficiency [7,8,30]. At ordinary temperatures, the small positive energy gaps do not suppress the efficiency of the QRVR transitions because the molecule can borrow energy from the translational motion. At ultracold temperatures, however, these transitions are energetically closed. Because neighboring j values have small negative energy gaps that allow QRVR transitions to take place, we should expect to see structure in the distribution of rate coefficients for the j values near a crossing point.

The cross sections have been obtained for $v=0-5$ and $j>100$ using the CS formulation. The calculations were converged to within a few percent for $v>0$ using basis sets restricted to $v-1\leqslant v'\leqslant v+1$ and $j-10\leqslant j'\leqslant j+10$. The zero-temperature rate coefficients are shown in Figs. 3–5. In Fig. 3, the state-to-state rate coefficients are plotted as a function of j for He+CO($v=0,j$) in the limit of zero temperature. The pure rotational deexcitation curves are smoothly varying with an upturn at j values near dissociation. The curves representing rovibrational transitions are peaked at the j values where vibrationally upward QRVR transitions first become energetically allowed. Because the efficiencies of rovibrational and pure rotational transitions are comparable in magnitude, these peaks will appear as "steps" in the total quenching rate coefficient distribution. Similar behavior was found in the state-to-state rate coefficients for H_2 and O_2. In the case of O_2, however, the efficiency of pure rotational relaxation was too large for the steps to be observed in the total quenching rate coefficient distribution [12]. Figure 4 shows the state-to-state curves for $v=1$. The rovibrational curves appear to have "holes" at the j values where the classically allowed QRVR transitions are energetically closed (i.e., at the crossing points in the boxed regions of Fig. 2). The magnitude of the rovibrational rate coefficient on either side of a hole is comparable to or greater than that of the pure rotational deexcitation rate coefficient. Therefore, when all of the possible deexcitation rate coefficients are added together, the distribution of total quenching rate coefficients will also appear to contain the holes. Figure 5 shows the total quenching rate coefficients as a function of v and j. The steps in the $v=0$ curve and the holes in the $v>0$ curves are labeled according to their QRVR propensity rule [30]. The figure shows that the holes tend to increase in size and shift downward in j as v is increased.

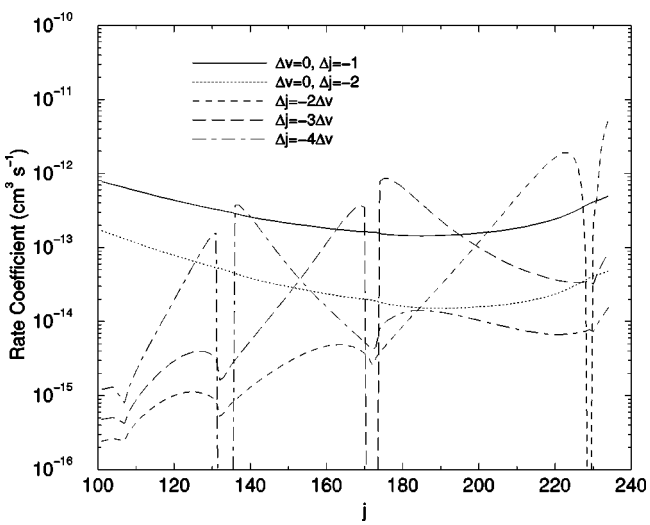

FIG. 4. State-to-state rate coefficients for He+CO($v=1,j$) in the limit of zero temperature. "Holes" occur at j values where QRVR transitions are energetically closed.

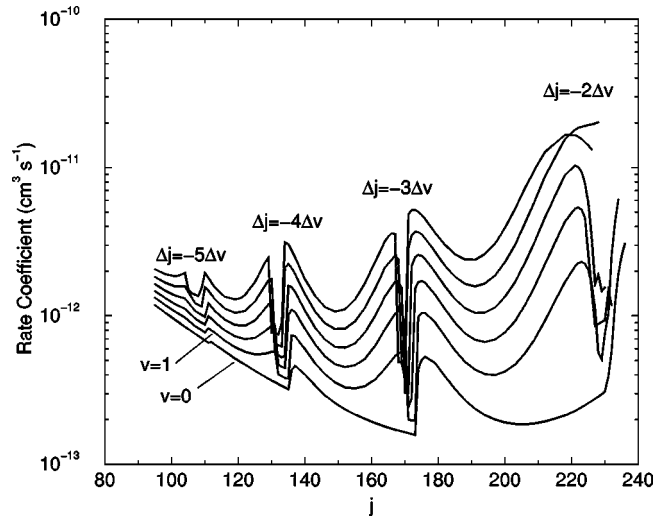

FIG. 5. Total quenching rate coefficients for He+CO(v,j) in the limit of zero temperature. The curves are given for $v=0,1,2,3,4,5$ and are increasing in order on the left side of the figure. The structures are labeled according to the nearest available QRVR transitions.

At j values very close to dissociation, we find an upturn in the zero-temperature rate coefficients with j (see Fig. 6). This behavior differs from the cases of H_2 and O_2 studied previously. In order to make sense of this result, we speculate that there may be a stronger competition between energy gap and angular momentum gap minimization for the present system. In previous work [12], it was shown that the rate coefficients followed an exponential energy gap fit. Here, we attempt to fit the numerical CS results using

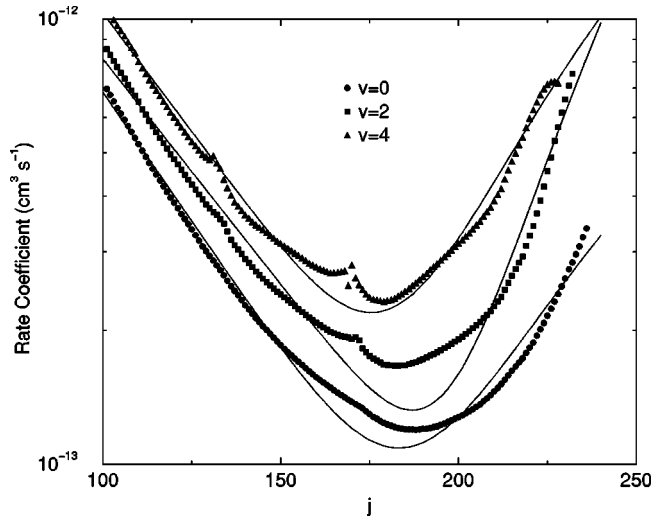

FIG. 6. Rate coefficients for $\Delta v=0$, $\Delta j=-1$ transitions in the limit of zero temperature. The solid lines attempt to fit the data using a balance between the energy and angular momentum gaps (see Table I).

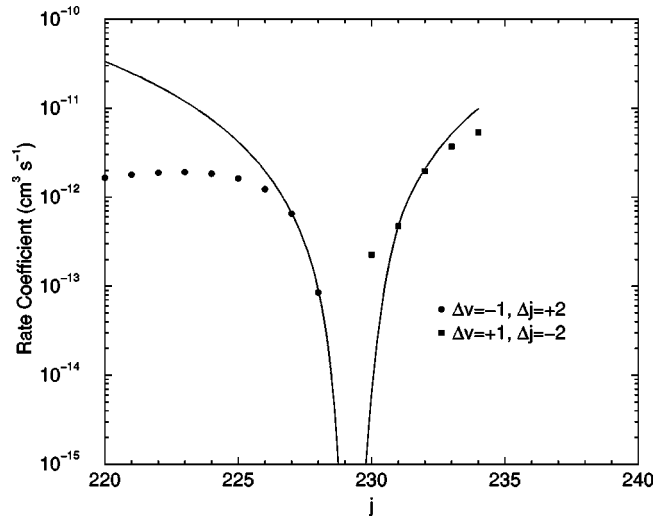

FIG. 7. Rate coefficients for $\Delta j=-2\Delta v$ transitions for He $+\mathrm{CO}(v=1,j)$ in the limit of zero temperature. The solid curves attempt to fit the data to the leading order behavior predicted by the Born approximation.

$$\Delta E \approx -\frac{j}{I} \quad \text{and} \quad \Delta|\vec{j}| \approx -1-\frac{1}{8j^2}$$

$$\Rightarrow \lim_{T\to 0} R(T) \approx c_1 \exp(-\alpha j) + c_2 \exp(-\beta/j^2) \tag{13}$$

with "best-fit" parameters given in Table I. The solid curves in Fig. 6 show that this type of balance between the energy and angular momentum gaps can give qualitative fits to the data. This situation is not entirely satisfactory, however, and we look for other ways to analyze the near dissociation data. One possibility is to apply the Born approximation. The Born approximation may be used when both the initial and final translational energies tend to zero. This situation can occur for transitions between states that have a very small energy gap. Figure 2 shows that the energy gaps for $\Delta j=-2\Delta v$ transitions are near zero when $v=1$ and $j\approx 230$. In this case, the leading order behavior of the zero-temperature rate coefficient is given by the Born approximation to be

$$\lim_{T\to 0} R(T) = O((\Delta E)^{5/2}). \tag{14}$$

Figure 7 shows the rate coefficients for $\Delta j=-2\Delta v$ transitions for $\mathrm{He}+\mathrm{CO}(v=1,j)$ in the limit of zero temperature. The solid curves attempt to fit the data to Eq. (14). Apart from one anomolous data point, it appears that the Born approximation is able to fit the data as the energy gap approaches zero. The anomolous data point at $j=230$ is most likely the result of a bound or virtual state of the three-body system that is too close to zero [31].

TABLE I. Fitting parameters for $\Delta v=0$, $\Delta j=-1$ rate coefficients in the limit of zero temperature: $R=c_1 \exp(-\alpha j)+c_2 \exp(-\beta/j^2)$.

v	c_1 (cm^3 s^{-1})	c_2 (cm^3 s^{-1})	α	β
0	9.80336×10^{-12}	6.67083×10^{-12}	0.026638	176777
1	9.15125×10^{-12}	3.08254×10^{-11}	0.025021	235517
2	8.32866×10^{-12}	2.54698×10^{-10}	0.023285	322256
3	8.40136×10^{-12}	5.24745×10^{-10}	0.022427	340188
4	1.19161×10^{-11}	2.54660×10^{-11}	0.024494	187721
5	2.16808×10^{-11}	2.51188×10^{-12}	0.028880	80936

The results presented above have been restricted to the limit of zero temperature. It would be interesting to see how the holes in the rate coefficient distributions become filled as the temperature is increased. Tabulation of temperature dependent rate coefficients for all values of v and j would require extensive computational effort and is not the path pursued here. Instead, we focus our attention on the $\Delta j=-3\Delta v$ hole that exists in the rate coefficient distribution for $v=1$ and j between 170 and 174 (see Fig. 5). In order to see how this hole in the distribution becomes filled as the temperature is increased, it is necessary to compute cross sections for a large range of translational energies. Figures 8–10 show the dominant energy-dependent cross sections multiplied by collision velocity in order to provide the dimensions of a rate coefficient. The curves in Figs. 8 and 9 are for the upward and downward QRVR transitions, whereas those in Fig. 10 are for the pure rotational transitions. The resonant structure in the cross sections that is seen in each curve occurs at energy values that are similar to those found at low rotational levels by Balakrishnan *et al.* [16] using the CC formulation. The translational energy range for resonances in weakly interacting atom-diatom systems, such as those involving helium, is not strongly affected by the internal diatomic state, so it is typical for these systems to possess a large number of resonances that are each associated with the same orbital angular momentum [32]. Figure 8 shows that the $j=170$ curve extends all the way to ultracold energies. Likewise, the $j=174$ curve in Fig. 9 is nonzero for the low energy limit. The approximate energies where the remaining curves become nonzero are indicated in the figures. Thermal rate coefficients may be obtained by convoluting the results

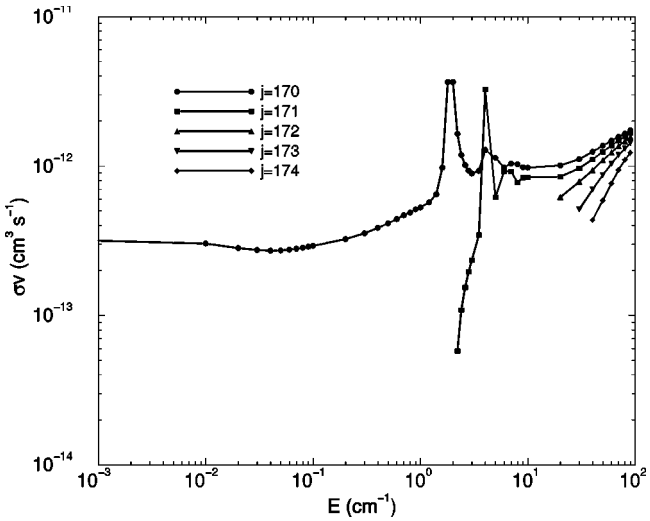

FIG. 8. Cross section times collision velocity for He+CO($v=1,j$) as a function of translational energy. The cross sections are for $\Delta v=-1$, $\Delta j=3$ transitions.

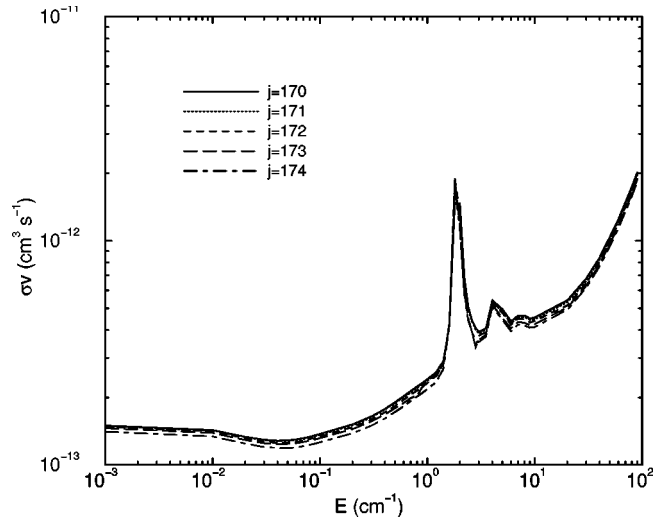

FIG. 10. Cross section times collision velocity for He+CO($v=1,j$) as a function of translational energy. The cross sections are for $\Delta v=0$, $\Delta j=-1$ transitions.

of Figs. 8–10 with a Maxwell-Boltzmann distribution of collision velocities as in Eq. (11). The results are given in Fig. 11 for several temperatures. The $T=0.1$ K curve nearly approaches the ultracold $T\rightarrow 0$ limit shown in Fig. 5. As temperature increases toward 1 K, the hole in the distribution begins to shrink. At $T=30$ K, the hole has completely disappeared and the distribution is smoothly varying with j. These results suggest that a buffer gas with a temperature of 300–500 mK would be sufficient to experimentally test the existence of such holes in the distribution of rate coefficients.

The present results also suggest that apart from odd-integer QRVR transitions that are allowed in heteronuclear systems, there does not appear to be any fundamental differences between homonuclear and heteronuclear diatomic relaxation at ultracold temperatures. Each system studied shows sharp structure in the state-to-state cross sections at j values where quasiresonant scattering is not allowed. Whether or not this structure appears in the total relaxation rate depends on the relative efficiency of the rovibrational and pure rotational deexcitation. For ultracold He+O_2, the pure rotational transitions are always dominant, whereas the total relaxation rates for ultracold helium collisions with H_2 and CO are strongly influenced by the rovibrational transitions. One important difference between homonuclear and heteronuclear systems is that heteronuclear polar molecules possess an electric dipole moment. The emitted radiation from such molecules would contain information about the collisions. Therefore, it should be possible to see evidence of

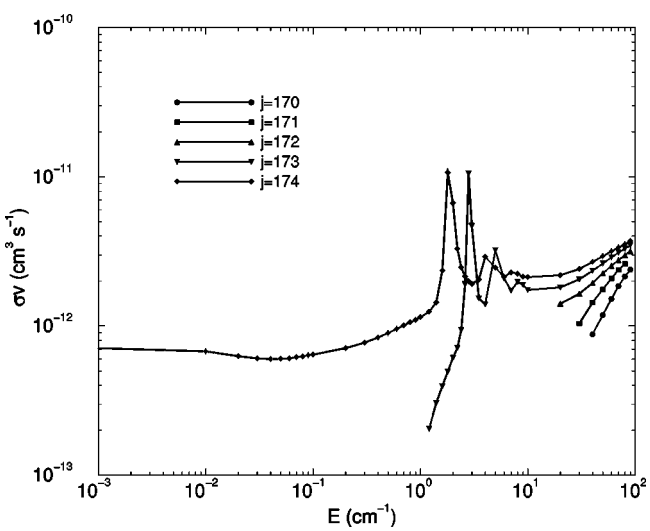

FIG. 9. Cross section times collision velocity for He+CO($v=1,j$) as a function of translational energy. The cross sections are for $\Delta v=1$, $\Delta j=-3$ transitions.

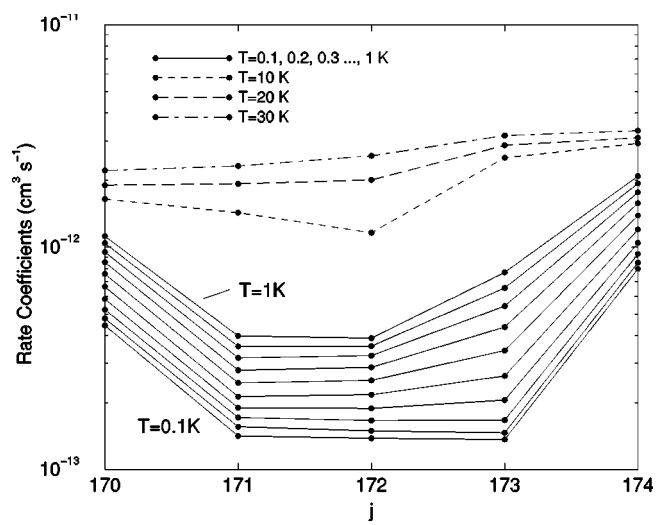

FIG. 11. Thermal rate coefficients for He+CO($v=1,j$) as a function of temperature and the five rotational levels shown in Figs. 8–10. The rate coefficients include deexcitation to all possible final states of CO. When $T>10$ K, the $\Delta j=-3\Delta v$ transitions are dominant for all five rotational levels. As the temperature is reduced below 1 K, these QRVR transitions become energetically closed for $j=171-173$ and the distribution of rate coefficients begins to approach the limiting ultracold result.

QRVR transitions and the associated j-dependent structure in the emission spectrum [33] for these systems.

IV. CONCLUSIONS

We have investigated cold and ultracold collisions involving rotationally excited CO molecules using CC, CS, and EP scattering formulations. Like in the cases of H_2 and O_2 studied previously [12], the decoupling approximations yield results that appear to be qualitatively correct as a function of the initial j level when j is larger than 20 or so. It is these large j values where the numerically exact CC method becomes too slow to be of any practical use. In cases where comparisons can be made, the decoupling approximations were found to be quantitatively accurate to within an overall factor of 2, which is acceptable considering the loss of accuracy introduced by a typical potential energy surface when applied to ultracold collisions. More importantly, the calculations reveal the presence of significant rovibrational transitions arising from QRVR energy transfer. These transitions give rise to sharp structure in the total quenching rate coefficients as a function of j. When QRVR transitions are energetically closed, the structure appears as a "hole" in the distribution of rate coefficients. The holes in the zero-temperature distributions were found to persist all the way up to temperatures that are typical of buffer gas cooling (e.g., 300–500 mK). Therefore, it should be possible to perform experimental tests of QRVR energy transfer using a buffer gas setup [13] without the need for magnetic trapping. A polar molecule such as CO would be an ideal candidate to perform such measurements due to the strong signal arising from the radiating electric dipole moment.

ACKNOWLEDGMENTS

This work was funded by the National Science Foundation, Grant Nos. PHY-0331073 and PHY-0244066.

[1] H. L. Bethlem, G. Berden, and G. Meijer, Phys. Rev. Lett. **83**, 1558 (1999).

[2] J. A. Maddi, T. P. Dinneen, and H. Gould, Phys. Rev. A **60**, 3882 (1999).

[3] H. L. Bethlem, G. Berden, A. J. A. van Roij, F. M. H. Crompvoets, and G. Meijer, Phys. Rev. Lett. **84**, 5744 (2000); H. L. Bethlem, G. Berden, F. M. H. Crompvoets, R. T. Jongma, A. J. A. van Roij, and G. Meijer, Nature (London) **406**, 491 (2000).

[4] J. Karczmarek, J. Wright, P. Corkum, and M. Ivanov, Phys. Rev. Lett. **82**, 3420 (1999).

[5] J. Li, J. T. Bahns, and W. C. Stwalley, J. Chem. Phys. **112**, 6255 (2000).

[6] D. M. Villeneuve, S. A. Aseyev, P. Dietrich, M. Spanner, M. Y. Ivanov, and P. B. Corkum, Phys. Rev. Lett. **85**, 542 (2000).

[7] R. C. Forrey, N. Balakrishnan, A. Dalgarno, M. Haggerty, and E. J. Heller, Phys. Rev. Lett. **82**, 2657 (1999).

[8] R. C. Forrey, N. Balakrishnan, A. Dalgarno, M. Haggerty, and E. J. Heller, Phys. Rev. A **64**, 022706 (2001).

[9] R. C. Forrey, Phys. Rev. A **63**, 051403 (2001).

[10] A. J. McCaffery, J. Chem. Phys. **113**, 10947 (2000).

[11] R. C. Forrey, Phys. Rev. A **66**, 023411 (2002).

[12] K. Tilford, M. Hoster, P. Florian, and R. C. Forrey, Phys. Rev. A **69**, 052705 (2004).

[13] J. M. Doyle, B. Friedrich, J. Kim, and D. Patterson, Phys. Rev. A **52**, R2515 (1995).

[14] J. D. Weinstein, R. deCarvalho, T. Guillet, B. Friedrich, and J. M. Doyle, Nature (London) **395**, 148 (1998).

[15] D. Egorov, T. Lahaye, W. Schollkopf, B. Friedrich, and J. M. Doyle, Phys. Rev. A **66**, 043401 (2002).

[16] N. Balakrishnan, A. Dalgarno, and R. C. Forrey, J. Chem. Phys. **113**, 621 (2000).

[17] C. Zhu, N. Balakrishnan, and A. Dalgarno, J. Chem. Phys. **115**, 1335 (2001).

[18] E. Bodo, F. A. Gianturco, and A. Dalgarno, Chem. Phys. Lett. **353**, 127 (2002).

[19] J. P. Reid, C. J. S. M. Simpson, and H. M. Quiney, Chem. Phys. Lett. **246**, 562 (1995); J. Chem. Phys. **107**, 9929 (1997); J. P. Reid and C. J. S. M. Simpson, Chem. Phys. Lett. **280**, 367 (1997).

[20] R. V. Krems, J. Chem. Phys. **116**, 4517 (2002); J. Chem. Phys. **116**, 4525 (2002).

[21] J. P. Reid, C. J. S. M. Simpson, H. M. Quiney, and J. M. Hutson, J. Chem. Phys. **103**, 2528 (1995).

[22] G. J. Wilson, M. L. Turnidge, A. S. Solodukhin, and C. J. S. M. Simpson, Chem. Phys. Lett. **207**, 521 (1993).

[23] A. M. Arthurs and A. Dalgarno, Proc. R. Soc. London, Ser. A **256**, 540 (1963).

[24] P. McGuire and D. J. Kouri, J. Chem. Phys. **60**, 2488 (1974); P. McGuire, *ibid.* **62**, 525 (1975).

[25] R. T. Pack, J. Chem. Phys. **60**, 633 (1974).

[26] H. Rabitz, J. Chem. Phys. **57**, 1718 (1972); G. Zarur and H. Rabitz, *ibid.* **59**, 943 (1973).

[27] J. M. Hutson and S. Green, MOLSCAT computer code, version 14 (1994), distributed by Collaborative Computational Project No. 6 of the Engineering and Physical Sciences Research Council (UK).

[28] T. G. A. Heijmen, R. Moszynski, P. E. S. Wormer, and A. van der Avoird, J. Chem. Phys. **107**, 9921 (1997).

[29] J. N. Murrel *et al.*, *Molecular Potential Energy Functions* (Wiley, New York, 1984).

[30] B. Stewart, P. D. Magill, T. P. Scott, J. Derouard, and D. E. Pritchard, Phys. Rev. Lett. **60**, 282 (1988); P. D. Magill, B. Stewart, N. Smith, and D. E. Pritchard, *ibid.* **60**, 1943 (1988).

[31] J. C. Flasher and R. C. Forrey, Phys. Rev. A **65**, 032710 (2002).

[32] R. C. Forrey, N. Balakrishnan, V. Kharchenko, and A. Dalgarno, Phys. Rev. A **58**, R2645 (1998).

[33] R. C. Forrey, Eur. Phys. J. D (2004), DOI 10.1140/epjd/e2004-00101-8.